Absorption and quantum coherence of a degenerate two-level system in the presence of a transverse magnetic field in different directions

He-bin Zhang,[1] Guoqing Yang,[1,2] Guang-ming Huang,[1] and Gao-xiang Li[1,*]
[1]*Department of Physics, Huazhong Normal University, Wuhan 430079, China*
[2]*School of Electronic and Information, Hangzhou Dianzi University, Hangzhou 310018, China*

(Received 11 December 2018; published 1 March 2019)

We investigate the absorption spectra for the $F_g = 1 \rightarrow F_e = 0$ transition of the D_2 line of ^{87}Rb excited by a linearly polarized light in the presence of a transverse magnetic field (TMF) in different directions. Using the theoretical methods in quantum optics, we obtain the analytical expressions for the atomic density-matrix elements and the absorption spectrum. We analyze the splitting proportional to the magnitude of the TMF in the coherent population trapping absorption spectrum and explain its physical origin. Then, the sensitivity of the resonance signal to the phase (in our case, to the angle between the TMF and the light polarization) is investigated. We show and explain the splitting of the bright resonance and find the simple dependence of the separation of this splitting on the magnitude and the direction of the TMF. Therefore, this system may provide a possible method for the measurement of the magnetic field vector. In addition, we study the coherence of the system based on an observable coherence measure, namely, robustness of coherence (ROC). We find that in the case where the absorption signal becomes difficult to detect, the change of the ROC spectrum becomes more obvious and the extreme points are well maintained. Therefore, this may provide a scheme for the measurement of the magnetic field which is complementary to that based on the absorption signal of the laser.

DOI: 10.1103/PhysRevA.99.033803

I. INTRODUCTION

Investigating the influence of a transverse magnetic field (TMF) [1] on the coherent resonance in alkali-metal atomic vapors is of great interest both in fundamental and application fields. In the degenerate two-level systems (DTLSs), a TMF drives the transition between the Zeeman sublevels, which leads to the redistribution of population and the establishment of coherences among the sublevels. In the so-called Hanle configuration [2,3], it has been found experimentally and theoretically that these processes can have significant impacts on the resonance signals of coherent population trapping (CPT) [1,4–10], electromagnetically induced transparency (EIT) [11–13], and electromagnetically induced absorption (EIA) [12–18]. The modifications of the magnitude, width, and shape of the resonance signals show a close dependence on the laser, ellipticity, and the magnitude of the TMF.

Some groups have reported that the coherent resonance signal can exhibit a splitting proportional to the magnitude of the TMF under specific experimental structures and conditions [1,4,8,13,19,20]. Margalit *et al.* [1] theoretically studied the effect of the TMF on the CPT resonance in both the Hanle and pump-probe configurations for the $F_g = 1 \rightarrow F_e = 0$ transition of the D_2 line of ^{87}Rb, and analytically derived the linear relationship between the splitting in the absorption spectrum and the TMF. For the same transition, Grewal *et al.* [8] showed that the linear relationship between the splitting and the TMF is preserved for both longitudinal and transverse scans, and discussed the effects of changing dissipation rates on this resonance signal according to the numerical results. Moreover, they experimentally observed this linear relationship in Hanle resonance for a $F_g = 2 \rightarrow F_e = 3$ transition of ^{87}Rb [19].

In addition, the effect of the TMF on the sign of the Hanle resonance is significant. It was reported that the dark (CPT,EIT) resonance can be transformed into the bright resonance for the $F_g \rightarrow F_e \leqslant F_g$ transition in the presence of the TMF [5–10]. For example, Yu *et al.* [6] observed a transformation from a CPT to a bright resonance with an increase of light ellipticity for the $F_g = 2 \rightarrow F_e = 1$ transition of ^{87}Rb in a buffer gas cell in the presence of a TMF. The corresponding theoretical study was reported by Noh and Moon [7]. Grewal *et al.* [8] theoretically discussed different magnetic-field scan geometries for the $F_g = 1 \rightarrow F_e = 0$ transition of the D_2 line of ^{87}Rb and found that as the ellipticity increases, the sign of the CPT resonance changes for a longitudinal scan and does not change for a transverse scan. Taskova *et al.* [9,10] reported a sign reversal of a CPT fluorescence caused by changing the laser power under the action of the TMF. Besides, for the $F_g \rightarrow F_e > F_g$ transition, it was also reported that the sign of resonance can be transformed from bright (ETA) into dark in the presence of the TMF depending on the laser power, ellipticity, or the angle between the TMF and the laser polarization [15–17].

Maybe due to the complexity of the realistic alkali-metal transition system in the present of the TMF, the theoretical analyses of most works are usually based on numerical solutions of the Bloch equation [3] or the Liouville equation [21,22] and there are very few analytical studies [1,13], so we believe that a detailed analytical discussion of a relevant problem is of general interest. We introduce the theoretical

*gaox@mail.ccnu.edu.cn

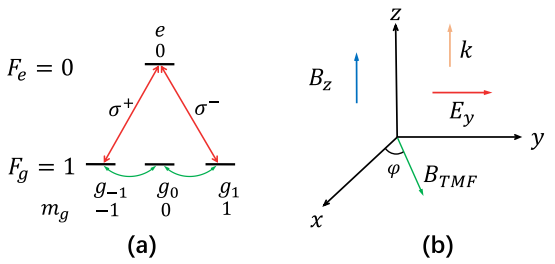

FIG. 1. (a) Atomic level configuration for the $F_g = 1 \rightarrow F_e = 0$ transition of the D_2 line of ^{87}Rb, and (b) longitudinal field scan configuration showing the directions of the the scanning magnetic field B_z, laser field wave vector (k), light polarization (E_y), and transverse magnetic field (B_{TMF})

methods in quantum optics to investigate the effect of the TMF on the absorption and the ground-state coherences in Hanle configuration. The physical origin of the splitting proportional to the magnitude of the TMF in the CPT spectrum [1,8] is explained analytically in detail. Further, we discuss the sensitivity of the resonance signal to the angle between the TMF and the light polarization, which leads to the sign reversal of the CPT resonance and the new splitting of the bright resonance.

In this paper, we investigate the absorption spectra of the $F_g = 1 \rightarrow F_e = 0$ transition of the D_2 line of ^{87}Rb excited by a linearly polarized light in the presence of a TMF in different directions. With the theoretical methods in quantum optics, the analytical expressions for the system are obtained in some appropriate approximations, and are in good agreement with the exact numerical results. Based on the analytical results, the physical origin of the splitting proportional to the magnitude of the TMF in the CPT absorption spectrum is explained. We demonstrate that when the TMF is perpendicular to the light polarization, the system is in a dark state modulated by the Zeeman splitting. Under the action of the ground-state relaxation processes (including the collisional and the transit processes), a part of the population can escape from the dark state, which leads to the absorption of the laser. Moreover, when the dark state of the system is modulated to the maximally coherent state [23] by scanning the longitudinal magnetic field, the impact of the collisional population redistribution on the dark state is minimum, which leads to the two dips in the absorption spectrum whose separation depends on the magnitude of the TMF. In addition, we explore the sensitivity of the resonance signal to the phase (in our case, to the angle between the TMF and the light polarization) originating from the closed-loop transition [24–29] as shown in Fig. 1(a). We find that the dark resonance can be transformed into a bright resonance as the angle changes. Moreover, in a certain angle range, the absorption spectrum of the bright resonance is also split and the two peaks correspond to the maximally mixed state in the subspace of the ground-state Zeeman sublevels. The maximally mixed state is immune to the effect of population redistribution caused by the ground-state relaxation processes, so the separation of the double peaks only depends on the magnitude and the direction of the TMF. This scheme may be used for the measurement of the magnetic field vector. Finally, we discuss the quantum coherence of the system based on an observable coherence measure, namely, robustness of coherence (ROC) [30,31]. Whether decreasing the collisional decay rates of the ground states or increasing the magnitude of the light field, the stability of the dark state of the system is enhanced, resulting in the absorption signal being difficult to detect. However, the change of the ROC spectrum becomes more obvious, and the extreme points are well maintained. In order to determine the magnitude of the magnetic field, one only need to find the separation of the two maxima. Therefore, this may provide a scheme for the measurement of the magnetic field which is complementary to that based on the absorption signal of the laser.

The paper is organized as follows. In Sec. II, the theoretical model is introduced. In Sec. III, we introduce the theoretical methods in quantum optics to solve the system analytically. Section IV is devoted to a discussion of the effect of the TMF in different directions on the absorption spectrum. In Sec. V, we explore the coherence of the system based on an observable coherence measure. The last section is a summary.

II. THEORETICAL MODEL

We consider the $F_g = 1 \rightarrow F_e = 0$ closed transition of the D_2 line of the ^{87}Rb excited by a linearly polarized light, so the system consists of a ground hyperfine state $F_g = 1$ composed of three Zeeman sublevels and an excited hyperfine state $F_e = 0$ composed of one Zeeman sublevel. The quantization axis (z axis) is set along the direction of propagation of the light beam, and the light polarization is taken along the y axis. In our system, the driving laser frequency ω is resonant with the atomic transition. A scanning magnetic field B_z, parallel to the direction of light propagation, causes the Zeeman splitting of the ground state. The additional transverse magnetic field B_{TMF}, in an arbitrary direction perpendicular to the laser field wave vector, is used to redistribute the population and create the coherences among the ground-state Zeeman sublevels, and we define the angle between the TMF and the x axis as φ [see Fig. 1(b)]. Within the rotating wave approximation, the total Hamiltonian of the system is given by

$$H' = H_0 + H_I' + H_B, \tag{1}$$

where H_0 is the unperturbed Hamiltonian

$$H_0 = \sum_{g_i} \omega_g |F_g, m_{g_i}\rangle\langle F_g, m_{g_i}| + \omega_e |F_e, m_e\rangle\langle F_e, m_e|, \tag{2}$$

and ω_g and ω_e represent the unperturbed energies of the ground and excited states, respectively. H_I' is the light-atom interaction Hamiltonian,

$$H_I' = \sum_{g_i} V_{eg_i} e^{-i\omega t} |F_e, m_e\rangle\langle F_g, m_{g_i}| + \mathrm{H.c.} \tag{3}$$

The interaction energy for the transition from level $|F_g, m_{g_i}\rangle$ to $|F_e, m_e\rangle$ can be evaluated using the Wigner-Eckart theorem [32,33],

$$\begin{aligned} V_{eg_i} &= -\langle F_e, m_e | \mathbf{d} | F_g, m_{g_i} \rangle \cdot \mathbf{E} \\ &= (-1)^{F_e - m_e + 1} \begin{pmatrix} F_e & 1 & F_g \\ -m_e & q & m_{g_i} \end{pmatrix} \Omega_L, \end{aligned} \tag{4}$$

where $\mathbf{d}$ is the electric dipole operator, $\mathbf{E}$ is the electric-field vector, and $\Omega_L = \langle F_e \parallel \mathbf{d} \parallel F_g\rangle E$ is the Rabi frequency of the light field. H_B is the total magnetic-field–atom interaction Hamiltonian consisting of the longitudinal magnetic-field–atom interaction Hamiltonian H_{B_z} and the TMF-atom interaction Hamiltonian $H_{B_{TMF}}$, that is,

$$H_B = H_{B_z} + H_{B_{TMF}}, \tag{5}$$

with

$$\begin{aligned} H_{B_z} &= \mu_B g_F \mathbf{F}\cdot\mathbf{B}_z \\ &= \Delta \sum_{g_i} \langle F_g, m_{g_i}|\mathbf{F}|F_g, m_{g_i}\rangle \cdot \mathbf{e}_0 |F_g, m_{g_i}\rangle\langle F_g, m_{g_i}|, \end{aligned} \tag{6}$$

where μ_B and g_F denote the Bohr magneton and the gyromagnetic factor of the ground state, respectively, and $\Delta = \mu_B g_F B_z$ is the Zeeman splitting of the ground state,

$$\begin{aligned} H_{B_{\mathrm{TMF}}} &= \mu_B g_F \mathbf{F}\cdot\mathbf{B}_{\mathrm{TMF}} \\ &= \Omega_T \sum_{g_i,g_j} \langle F_g, m_{g_i}|\mathbf{F}|F_g, m_{g_j}\rangle \cdot \mathbf{e}_T |F_g, m_{g_i}\rangle\langle F_g, m_{g_j}|, \end{aligned} \tag{7}$$

where $\mathbf{e}_T = \cos\varphi \mathbf{e}_x + \sin\varphi \mathbf{e}_y = \frac{1}{\sqrt{2}}(-e^{-i\varphi}\mathbf{e}_+ + e^{i\varphi}\mathbf{e}_-)$ is the unit vector of the TMF with $\mathbf{e}_\pm = \mp(\mathbf{e}_x \pm i\mathbf{e}_y)$ [22], $\Omega_T = \mu_B g_F B_{\mathrm{TMF}}$ is the Larmor frequency of the TMF.

Because the driving laser field is resonant with the atomic transition in our system, the Hamiltonian of the system in the frame rotating at the driving laser frequency ω is then given by

$$H = H_I + H_B, \tag{8}$$

with

$$H_I = \sum_{g_i} V_{eg_i} |F_e, m_e\rangle\langle F_g, m_{g_i}| + \mathrm{H.c.} \tag{9}$$

For later convenience we denote $|F_g, m_{g_i}\rangle \equiv |g_i\rangle$ and $|F_e, m_e\rangle \equiv |e\rangle$. The master equation of the atomic density matrix ρ takes the form

$$\dot{\rho} = -i[H, \rho] + \mathcal{L}_e\rho + \mathcal{L}_{\mathrm{transfer}}\rho + \mathcal{L}_{\mathrm{transit}}\rho, \tag{10}$$

where

$$\mathcal{L}_e\rho = \sum_{i=-1}^{1} \frac{\Gamma_i}{2} D[\sigma_{g_i e}] + \Gamma^* D[\sigma_{ee}], \tag{11}$$

$$\mathcal{L}_{\mathrm{transfer}}\rho = \sum_{g_i,g_j} \frac{\Gamma_{g_i g_j}}{2} D[\sigma_{g_i g_j}]. \tag{12}$$

Here the $D[\sigma_{mn}] \equiv 2\sigma_{mn}\rho\sigma_{nm} - \rho\sigma_{nm}\sigma_{mn} - \sigma_{nm}\sigma_{mn}\rho$ is the Lindblad superoperator with $\sigma_{mn} \equiv |m\rangle\langle n|$. Γ_i represents the decay rate from atomic excited state $|e\rangle$ to the ground state $|g_i\rangle$, and Γ^* is the rate of the phase-changing collisions. The rate of the collisional transfer from the ground-state sublevels $|g_i\rangle$ to $|g_j\rangle$ is given by $\Gamma_{g_i g_j}$ [34], which is uniformly represented as Γ_g in our system.

As we can see, the above part of the master equation is a standard Lindblad form [35,36]. However, we also need to consider the effect of the transit relaxation and repopulation for the atomic vapor subject to a laser beam. These processes can be written phenomenologically as [22]

$$\mathcal{L}_{\mathrm{transit}}\rho = -\tfrac{1}{2}\{R, \rho\} + \Lambda. \tag{13}$$

The first term denotes the transit relaxation due to the exit of atoms from the laser beam and the corresponding relaxation matrix is given by

$$R = \gamma \begin{pmatrix} 1 & 0 & 0 & 0 \\ 0 & 1 & 0 & 0 \\ 0 & 0 & 1 & 0 \\ 0 & 0 & 0 & 1 \end{pmatrix}, \tag{14}$$

where γ denotes the transit decay rate due to the atoms flying through the laser beam. The second term Λ describes the repopulation due to the atoms arriving in the beam, and is given by

$$\Lambda = \gamma \begin{pmatrix} \rho_{g_1 g_1}^{eq} & 0 & 0 & 0 \\ 0 & \rho_{g_0 g_0}^{eq} & 0 & 0 \\ 0 & 0 & \rho_{g_{-1} g_{-1}}^{eq} & 0 \\ 0 & 0 & 0 & \rho_{ee}^{eq} \end{pmatrix}, \tag{15}$$

where ρ_{ii}^{eq} represents the equilibrium population of state $|i\rangle (i = g_1, g_0, g_{-1}, e)$ in the absence of the driving laser field.

We note that the expansion of the master equation, Eq. (10), is equivalent to the optical Bloch equations used in Ref. [1]. Although this equation can be solved numerically under steady-state conditions, it is difficult to obtain the analytical solution of the system directly. Therefore, we will simplify the master equation of the atomic density matrix based on some appropriate approximations in the following section.

III. GENERAL SOLUTION FOR THE MASTER EQUATION

In our system, the decay rates of the excited state are much greater than the magnitude of the laser and the dissipation rates of the ground states, i.e., $\Gamma_i, \Gamma^* \gg |V_{eg_i}|, \Gamma_g, \gamma$. This condition implies that light-atom interaction Hamiltonian H_I can be treated as a weak perturber to the system and the degrees of freedom of the excited state can be adiabatically eliminated using the second-order perturbation theory [21,37,38]. Therefore, the motion equation for the reduced density matrix ρ_g of the ground-state Zeeman sublevels can be reexpressed as the form

$$\dot{\rho}_g = -i[H_B, \rho_g] + \mathcal{L}_{\mathrm{transfer}}\rho_g + \mathcal{L}'_{\mathrm{transit}}\rho_g + \mathcal{L}_{\mathrm{laser}}\rho_g, \tag{16}$$

where

$$H_B = H_{B_z} + H_{B_{\mathrm{TMF}}}, \tag{17}$$

$$\mathcal{L}'_{\mathrm{transit}}\rho_g = -\frac{1}{2}\{R', \rho_g\} + \Lambda', \tag{18}$$

$$\mathcal{L}_{\mathrm{laser}}\rho_g = \sum_{p,i,j,} \frac{1}{2}\Gamma_{p,i,j,p}(2\sigma_{g_p g_i}\rho_g\sigma_{g_j g_p} - \rho_g\sigma_{g_j g_i} - \sigma_{g_j g_i}\rho_g). \tag{19}$$

Here, R' and Λ' are, respectively, the truncated form of the transit relaxation operator R and the repopulation operator Λ in the subspace of the ground-state Zeeman sublevels. $\mathcal{L}_{\mathrm{laser}}\rho_g$ denotes the effects of the laser-induced population

redistribution and the dephasing generated by eliminating the excited state adiabatically and consists of 12 terms, with the corresponding equivalent dissipation rate $\Gamma_{p,i,j,p} = \frac{4\Gamma_p V_{eg_i} V_{g_j e}}{(\Gamma_1+\Gamma_0+\Gamma_{-1})(\Gamma_1+\Gamma_0+\Gamma_{-1}+2\Gamma^*)}$ ($p = 0, \pm 1$ and $i, j = \pm 1$) which can be uniformly represented as Γ_L in our system. In addition, the dynamic evolution of the excited state can be obtained by

$$\begin{aligned}
\rho_{eg_1} &= -\frac{2i\left(V_{eg_1}\rho_{g_1g_1} + V_{eg_{-1}}\rho_{g_{-1}g_1}\right)}{\Gamma_1+\Gamma_0+\Gamma_{-1}+2\Gamma^*},\\
\rho_{eg_0} &= -\frac{2i\left(V_{eg_1}\rho_{g_1g_0} + V_{eg_{-1}}\rho_{g_{-1}g_0}\right)}{\Gamma_1+\Gamma_0+\Gamma_{-1}+2\Gamma^*},\\
\rho_{eg_{-1}} &= -\frac{2i\left(V_{eg_1}\rho_{g_1g_{-1}} + V_{eg_{-1}}\rho_{g_{-1}g_{-1}}\right)}{\Gamma_1+\Gamma_0+\Gamma_{-1}+2\Gamma^*},\\
\rho_{ee} &= \frac{4\left(V_{eg_1}V_{g_1e}\rho_{g_1g_1} + V_{eg_1}V_{g_{-1}e}\rho_{g_1g_{-1}} + V_{eg_{-1}}V_{g_1e}\rho_{g_{-1}g_1} + V_{eg_{-1}}V_{g_{-1}e}\rho_{g_{-1}g_{-1}}\right)}{(\Gamma_1+\Gamma_0+\Gamma_{-1})(\Gamma_1+\Gamma_0+\Gamma_{-1}+2\Gamma^*)}.
\end{aligned} \tag{20}$$

To explore the influence of the TMF on the Hanle absorption conveniently, we study the system in the dressed-atomic-state representation. The dressed states, defined as the eigenstates of the Hamiltonian H_B, are given by [39]

$$\begin{aligned}
|a\rangle &= \frac{1+\epsilon}{2}e^{-i\varphi}|g_1\rangle + \frac{\eta}{\sqrt{2}}|g_0\rangle + \frac{1-\epsilon}{2}e^{i\varphi}|g_{-1}\rangle,\\
|b\rangle &= \frac{\eta}{\sqrt{2}}e^{-i\varphi}|g_1\rangle - \epsilon|g_0\rangle - \frac{\eta}{\sqrt{2}}e^{i\varphi}|g_{-1}\rangle,\\
|c\rangle &= \frac{1-\epsilon}{2}e^{-i\varphi}|g_1\rangle - \frac{\eta}{\sqrt{2}}|g_0\rangle + \frac{1+\epsilon}{2}e^{i\varphi}|g_{-1}\rangle,
\end{aligned} \tag{21}$$

with $\epsilon = \frac{\Delta}{\Omega}$, $\eta = \frac{\Omega_T}{\Omega}$, $\Omega = \sqrt{\Delta^2+\Omega_T^2}$. In the dressed-state representation, the Hamiltonian H_B becomes the following diagonal form:

$$H^{(D)} = \begin{pmatrix} \omega_a & 0 & 0\\ 0 & \omega_b & 0\\ 0 & 0 & \omega_c \end{pmatrix}, \tag{22}$$

with $\omega_a = \Omega$, $\omega_b = 0$, $\omega_c = -\Omega$, where ω_m denotes the energy of the dressed state $|m\rangle$. In addition, for later convenience we rewrite the laser-atom interaction Hamiltonian in the dressed-state representation as

$$H_I^{(D)} = V_{ea}|e\rangle\langle a| + V_{eb}|e\rangle\langle b| + V_{ec}|e\rangle\langle c| + \text{H.c.}, \tag{23}$$

where the light-atom interaction energy of the transition from the ground state $|m\rangle$ ($m = a, b, c$) to the excited state $|e\rangle$ are given by

$$\begin{aligned}
V_{ea} &= \frac{1+\epsilon}{2}V_{eg_1}e^{-i\varphi} + \frac{1-\epsilon}{2}V_{eg_{-1}}e^{i\varphi},\\
V_{eb} &= \frac{\eta}{\sqrt{2}}\left(V_{eg_1}e^{-i\varphi} - V_{eg_{-1}}e^{i\varphi}\right),\\
V_{ec} &= \frac{1-\epsilon}{2}V_{eg_1}e^{-i\varphi} + \frac{1+\epsilon}{2}V_{eg_{-1}}e^{i\varphi}.
\end{aligned} \tag{24}$$

When $\Omega \gg \Gamma_g, \gamma$, one can apply the secular approximation [37,40] to simplify the equations of motion for the ground states in the dressed-state representation, which reduce to the rate-equation form:

$$\begin{aligned}
\dot{\rho}_{aa} &= -(R_{ab}+R_{ac})\rho_{aa} + R_{ca}\rho_{cc} + R_{ba}\rho_{bb} - \gamma\left(\rho_{aa} - \rho_{aa}^{eq}\right),\\
\dot{\rho}_{bb} &= -(R_{bc}+R_{ba})\rho_{bb} + R_{cb}\rho_{cc} + R_{ab}\rho_{aa} - \gamma\left(\rho_{bb} - \rho_{bb}^{eq}\right),\\
\dot{\rho}_{cc} &= -(R_{ca}+R_{cb})\rho_{cc} + R_{ac}\rho_{aa} + R_{bc}\rho_{bb} - \gamma\left(\rho_{cc} - \rho_{cc}^{eq}\right).
\end{aligned} \tag{25}$$

Here $R_{mn}(m, n = a, b, c)$ represents the atomic transition rate from $|m\rangle$ to $|n\rangle$ as demonstrated in Fig. 2, and can be expressed in the following form:

$$\begin{aligned}
R_{ab} &= R_{cb} = R_L^{\text{in}} + R_g^{\text{col}},\\
R_{ba} &= R_{bc} = R_L^{\text{out}} + R_g^{\text{col}},\\
R_{ac} &= R_{ca} = R_L^{\text{in}} + \frac{1}{8}\Gamma_g(5 + 6\epsilon^2 - 3\epsilon^4),
\end{aligned} \tag{26}$$

with

$$\begin{aligned}
R_L^{\text{in}} &= \tfrac{1}{2}\Gamma_L(1 + \epsilon^2 + \eta^2\cos 2\varphi),\\
R_L^{\text{out}} &= \Gamma_L\eta^2(1 - \cos 2\varphi),\\
R_g^{\text{col}} &= \tfrac{1}{4}\Gamma_g(3 - 2\epsilon^2 + 3\epsilon^4),
\end{aligned} \tag{27}$$

where R_L^{in} represents the rate of the laser-induced transitions from $|a\rangle$ to $|b\rangle$ and from $|c\rangle$ to $|b\rangle$, R_L^{out} represents the rate of the laser-induced transitions from $|b\rangle$ to $|a\rangle$ and from $|b\rangle$ to $|c\rangle$, and R_g^{col} represents the rate of the collisional population redistribution between $|a\rangle$ or $|c\rangle$ and $|b\rangle$.

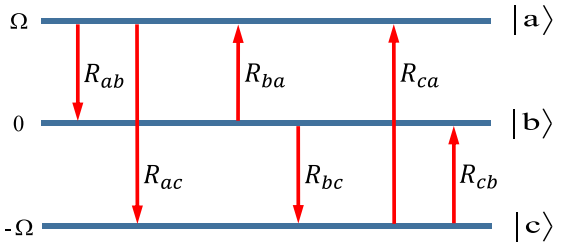

FIG. 2. Diagram of atomic dressed states and dressed-state transitions.

By solving Eq. (25), the steady-state solutions of the dressed-state populations are given by

$$\rho_{aa} = \rho_{cc} = \frac{3R_{ba} + \gamma}{3(R_{ab} + 2R_{ba} + \gamma)}, \qquad \rho_{bb} = 1 - 2\rho_{aa}. \tag{28}$$

Thus, we can obtain the population difference between the dressed state $|b\rangle$ and $|a\rangle$ ($|c\rangle$) as

$$W = \frac{3\left(R_L^{\text{in}} - R_L^{\text{out}}\right)}{3(R_{ab} + 2R_{ba} + \gamma)}. \tag{29}$$

Obviously, we can see that the population distribution in the dressed-state representation is completely determined by the rates of the laser-induced transitions into and out of the state $|b\rangle$, the collisional population redistribution, and the transit effect. The elements of the density matrix of the ground states in the bare-state representation are given by

$$\begin{aligned} \rho_{g_1g_1} &= \rho_{g_{-1}g_{-1}} = \frac{\eta^2}{2} + \frac{3\epsilon^2 - 1}{2}\rho_{aa}, \\ \rho_{g_0g_0} &= 1 - 2\rho_{g_1g_1}, \\ \rho_{g_1g_0} &= \frac{\epsilon\eta}{\sqrt{2}}(3\rho_{aa} - 1)e^{-i\varphi}, \\ \rho_{g_1g_{-1}} &= \frac{\eta^2}{2}(3\rho_{aa} - 1)e^{-2i\varphi}, \\ \rho_{g_0g_{-1}} &= -\rho_{g_1g_0}. \end{aligned} \tag{30}$$

Therefore, according to Refs. [41,42], the Hanle absorption spectrum can be written in the dressed-state representation as

$$\alpha = \frac{2}{(\Gamma + 2\Gamma^*)\Gamma_L}\left(\rho_{aa}R_L^{\text{in}} + \rho_{bb}R_L^{\text{out}} + \rho_{cc}R_L^{\text{in}}\right). \tag{31}$$

Within the adiabatic approximation and the secular approximation, we can see that the form of the absorption spectrum becomes compact, and the physical significance is evident. The expression includes only three absorption components which correspond to the three transitions driven by the laser field [see Eq. (24)], and all cross terms vanish. In order to facilitate the following discussion, we refer to these three terms as *a*-, *b*-, and *c*-absorption channel, respectively.

IV. HANLE ABSORPTION

A. Case of $\varphi = 0^o$

We first consider the case where the TMF is perpendicular to the light polarization, i.e., $\varphi = 0^\circ$. In Fig. 3, we show the numerical and analytical results for the Hanle absorption as a function of the Zeeman splitting. We note that the CPT dip in the presence of the TMF is widened compared with that in the absence of the TMF. However, the most significant feature in the figures is the splitting of the CPT dip, which results in a double dips structure of the absorption spectrum. And with different dissipation rates of the ground states, this structure remains though the amplitude of the absorption changes. The separation of the splitting is proportional to the magnitude of the TMF, which has been pointed out and discussed for the same transition [1,8]. In order to gain greater insight into the physical origin of the splitting in the absorption spectrum,

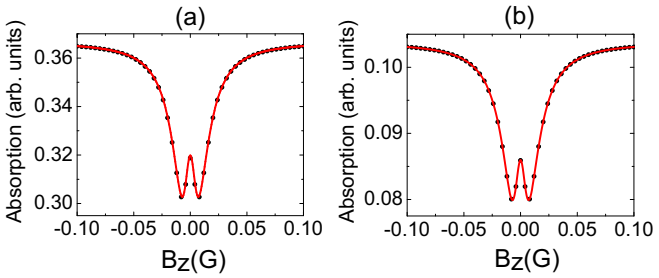

FIG. 3. Hanle absorption plotted as a function of the Zeeman splitting, for $\Omega_L = 6\pi \times 10^6\ \text{s}^{-1}$, $B_{\text{TMF}} = 0.1$ G, $\Gamma^* = 100\Gamma$, $\Gamma = 2\pi \times 6$ MHz, $\gamma = \Gamma_g$, and (a) $\Gamma_g = 10^{-5}\Gamma$, (b) $\Gamma_g = 0.2 \times 10^{-5}\Gamma$. The red solid line and the black solid dots represent the analytical and numerical results, respectively.

we will explore this phenomenon according to the analytical expressions for the system obtained in Sec. III.

For $\varphi = 0^\circ$, it is evident that $H|b\rangle = 0$, which denotes that the dressed state $|b\rangle$ is a so-called dark state [43,44]. According to Eqs. (26) and (27), the rates of the transitions between $|a\rangle$ or $|c\rangle$ and $|b\rangle$ can be reduced to the following form:

$$\begin{aligned} R_{ab}^{(0)} &= R_{cb}^{(0)} = R_L^{\text{in}(0)} + R_g^{\text{col}}, \\ R_{ba}^{(0)} &= R_{bc}^{(0)} = R_L^{\text{out}(0)} + R_g^{\text{col}}, \end{aligned} \tag{32}$$

with

$$\begin{aligned} R_L^{\text{in}(0)} &= \Gamma_L, \\ R_L^{\text{out}(0)} &= 0. \end{aligned} \tag{33}$$

Therefore, we can obtain the dress-state populations according to Eqs. (28) and (32) as

$$\rho_{aa}^{(0)} = \rho_{cc}^{(0)} = \frac{1}{3}\left(1 - \frac{\Gamma_L}{3R_g^{\text{col}} + \Gamma_L + \gamma}\right), \qquad \rho_{bb}^{(0)} = 1 - 2\rho_{aa}^{(0)}. \tag{34}$$

From Eq. (33), we see that the rates of the laser-induced transitions from $|a\rangle$ to $|b\rangle$ and from $|c\rangle$ to $|b\rangle$ reach the maximum due to the completely constructive interference, and the rates of the laser-induced transitions from $|b\rangle$ to $|a\rangle$ and from $|b\rangle$ to $|c\rangle$ vanish due to the completely destructive interference. Therefore, when the ground-state relaxation processes caused by the collisional and transit terms in Eqs. (12) and (13) are ignored, that the dark state $|b\rangle$ is completely decoupled from the system so that all the population is trapped into $|b\rangle$ [see Eq. (34)]. In general, when the ground-state relaxation processes are included, the population difference between the dressed states $|b\rangle$ and $|a\rangle$ ($|c\rangle$) takes the form of

$$W^{(0)} = \frac{\Gamma_L}{3R_g^{\text{col}} + \Gamma_L + \gamma}. \tag{35}$$

It is evident that the population trapped in the dark state $|b\rangle$ is always more than that in other states. The bare-state populations can also be easily obtained according to Eqs. (30) and (34). In Fig. 4, we show the dressed-state and the

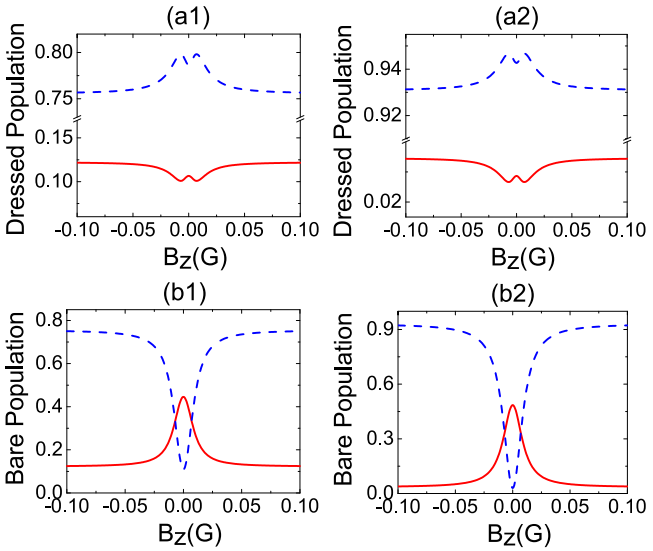

FIG. 4. The dressed-state and the bare-state populations of the ground-state Zeeman sublevels plotted as a function of the Zeeman splitting for (a1) and (b1) $\Gamma_g = 10^{-5}\Gamma$, (a2) and (b2) $\Gamma_g = 0.2 \times 10^{-5}\Gamma$, $\gamma = \Gamma_g$, and the other parameters are the same as in Fig. 3. The red solid line represents the populations of the state $|a\rangle$ ($|c\rangle$) in frame (a), and $|g_1\rangle$ ($|g_{-1}\rangle$) in frame (b), respectively; the blue dashed line represents the populations of the state $|b\rangle$ in frame (a), and $|g_0\rangle$ in frame (b), respectively.

bare-state population distributions for the same parameters as in Fig. 3 according to the above expressions, and they agree perfectly with the numerical exact solutions (not shown).

It is worth noting that for different Zeeman splittings, the quantum state $|b\rangle = \frac{\eta}{\sqrt{2}}e^{-i\varphi}|g_1\rangle - \epsilon|g_0\rangle - \frac{\eta}{\sqrt{2}}e^{i\varphi}|g_{-1}\rangle$ remains a dark state, despite the change of the specific form. In other words, we get a dark state modulated by the Zeeman splitting Δ. However, under the effect of the ground-state relaxation processes, some of the population is transferred from the dark state $|b\rangle$ to the bright states $|a\rangle$ and $|c\rangle$. According to Eq. (34), the amount of the population transferred depends on the ratio of the rates of collisional population redistribution and the transit effect to that of the laser-induced transitions into the dark state $|b\rangle$. Meanwhile, when scanning the Zeeman splitting Δ, the change of the population distribution is completely determined by the change of the rate of the collisional population redistribution $R_g^{\rm col}$.

For $\Delta = \pm\Omega_T/\sqrt{2}$, the dark state $|b\rangle = \frac{1}{\sqrt{3}}(|g_1\rangle \mp |g_0\rangle - |g_{-1}\rangle)$ is also the maximally coherent state, in which the three Zeeman sublevels $|g_1\rangle$, $|g_0\rangle$, and $|g_{-1}\rangle$ have the equal probability amplitudes. Therefore, the population is equally distributed among the three Zeeman sublevels even though the effect of the population redistribution caused by the ground-state relaxation processes is included [see Fig. 4(b)]. And, according to Eq. (27), the impact of the collisional population redistribution on the dark state $|b\rangle$ is minimum at these points. In this case, the deviation of the system from the dark state $|b\rangle$ has minima, which causes the populations in the dressed states $|b\rangle$ and $|a\rangle$($|c\rangle$) to reach a maximum and minimum, respectively, as shown in Fig. 4(a). For $\Delta = 0$, the dark state $|b\rangle = \frac{1}{\sqrt{2}}(|g_1\rangle - |g_{-1}\rangle)$ does not consist of the sublevel $|m = 0\rangle$. Therefore, the impact of the collisional population redistribution on the dark state is maximum, which causes the populations in the dressed states $|b\rangle$ and $|a\rangle$ ($|c\rangle$) to reach a minimum and maximum, respectively, as shown in Fig. 4(a).

The absorption spectrum can be found from Eq. (31) to be

$$\alpha^{(0)} = \frac{2}{\Gamma_L(\Gamma + 2\Gamma^*)} R_L^{in(0)}\left(\rho_{aa}^{(0)} + \rho_{cc}^{(0)}\right). \tag{36}$$

We see that since the state $|b\rangle$ is a dark state, the b-absorption channel is turned off and only a- and c-absorption channels remain. Under the effect of the ground-state relaxation processes, some of the population is transferred from the dark state $|b\rangle$ to the bright states $|a\rangle$ and $|c\rangle$, which results in the absorption of the laser. Due to the completely constructive interference, the rate of the laser-induced transitions into the dark state $|b\rangle$ reaches and remains a maximum, i.e., $R_L^{\rm in(0)} = \Gamma_L$, so that the shape of the absorption spectrum is totally determined by the populations in the dressed states $|a\rangle$ and $|c\rangle$ [see Eq. (36)]. Meanwhile, since the population in the ground states is conserved, we can also think that the absorption is determined by the population trapped in the dark state $|b\rangle$. Therefore, a corresponding relationship is established between the absorption signal and the specific form of the dark state $|b\rangle$ in our system.

As we have mentioned above, at $\Delta = \pm\Omega_T/\sqrt{2}$, the dark state $|b\rangle$ is also the maximally coherent state and the population is equally distributed among the three Zeeman sublevels, so the impact of the collisional population redistribution on the dark state $|b\rangle$ is minimum. In this case, the populations in the dressed states $|a\rangle$ and $|c\rangle$ reach minima, so that the absorption has minima (see Fig. 3). This phenomenon can be used in magnetometry as proposed by Ref. [1]. At $\Delta = 0$, the sublevel $|m = 0\rangle$ is not included in the dark state $|b\rangle$, so the impact of the collisional population redistribution on the dark state reaches a minimum. In this case, the populations in the dressed states $|a\rangle$ and $|c\rangle$ reach maxima, so that the absorption has a maximum.

Since the populations in the states $|a\rangle$ and $|c\rangle$ are determined by the ratio of the rates of collisional population redistribution and the transit effect to that of the laser-induced transitions [see Eq. (34)], the amplitude of the absorption are also determined by this ratio. When the magnitude of the laser is constant, the smaller Γ_g, γ, the weaker the absorption (see Fig. 3). Evidently, when the population redistribution caused by the ground-state relaxation processes disappears, i.e., Γ_g, $\gamma = 0$, the absorption spectrum becomes zero since the population is completely accumulated in the dark state $|b\rangle$ modulated by the Zeeman splitting. Meanwhile, the visibility of the splitting of the absorption spectrum depends on the ratio of the rate of the collisional population redistribution to that of the laser-induced transitions and the transit effect [also see Eq. (34)]. When this ratio is small, the splitting will become indiscernible, which limits the applicability of this scheme to the measurement of the magnetic field. In this case however, if the coherence of the system is measured, the limitation can be broken. (This point will be discuss in detail in Sec. V.)

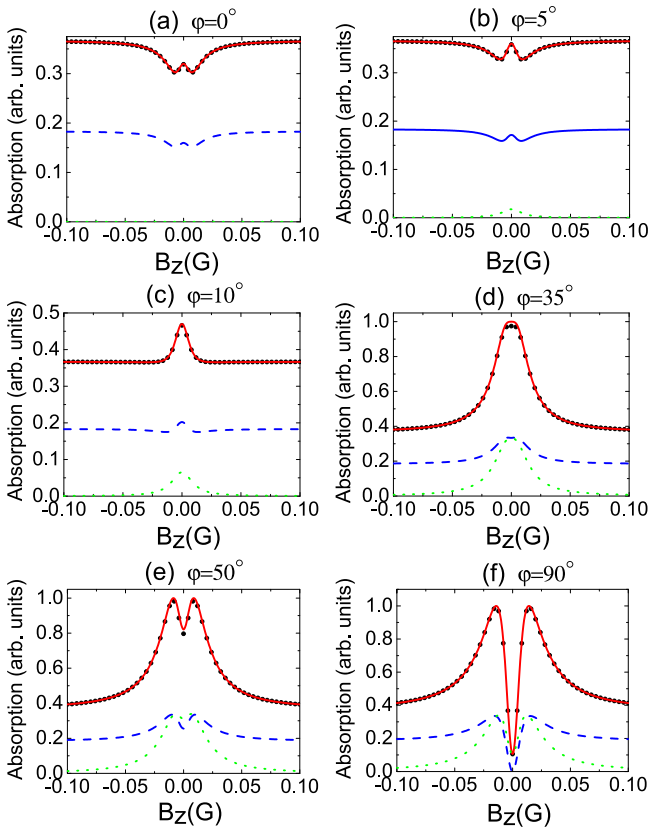

FIG. 5. Hanle absorption plotted as a function of the Zeeman splitting. For (a)–(f) $\varphi = 0^\circ, 5^\circ, 10^\circ, 35^\circ, 50^\circ, 90^\circ$ and the other parameters are the same as in Fig. 3(a). The red solid lines and the black solid dots represent, respectively, the analytical and numerical results of the total Hanle absorption. The the blue dashed line and the green dotted line represent, respectively, the absorption components of the a (c) and b-absorption channels.

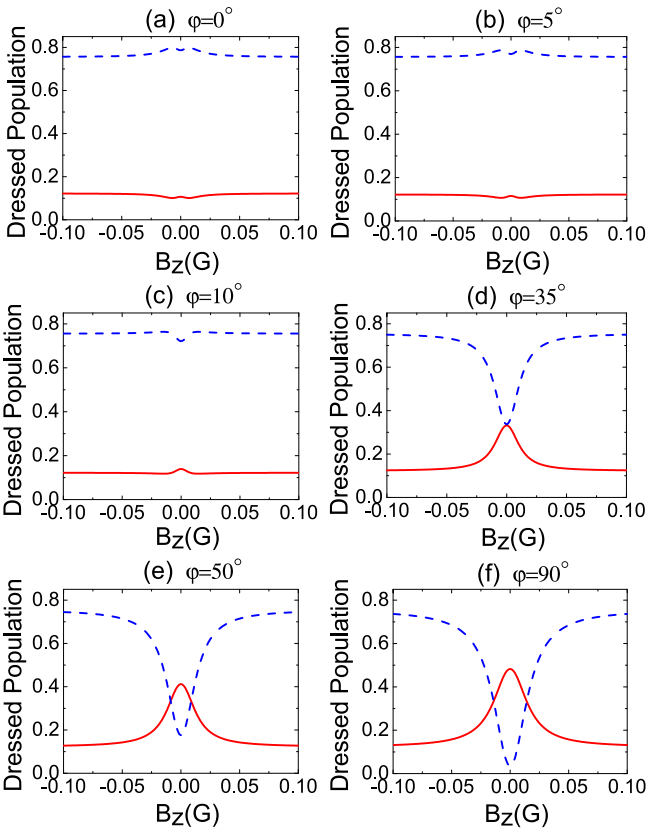

FIG. 6. The dress-state populations of the ground-state Zeeman sublevels plotted as a function of the the Zeeman splitting. The parameters are the same as in Fig. 5. The red solid line and the blue dotted line, respectively, represent the populations in the dressed states $|a\rangle$ ($|c\rangle$) and $|b\rangle$.

B. Case of arbitrary φ

We next consider the case where the angle φ between the TMF and the light polarization is changed. In our system, the TMF and the linearly polarized light drive a closed-loop transition [see Fig. 1(a)], where the resonance signal is sensitive to the phase (in our case, the angle between the TMF and the light polarization). Therefore, we investigate the effect of changing the angle between the TMF and the light polarization on the Hanle absorption. In Fig. 5, we show the absorption spectra with different angles. The red solid lines represent the analytical results according to Eq. (31), and the black solid dots represent the exact numerical results. Obviously, our analytical results are in good agreement with the numerical results. It can be seen that as the angle φ increases, the center peak rises and the two dips gradually disappear, so that the CPT dark resonance is transformed into the bright resonance. Remarkably, this transformation is not the same as the previous one [5–10], in which the change in the ellipticity of the laser is indispensable. Here, we only need to change the angle φ between the TMF and the light polarization. Furthermore, from Fig. 5 we see that the splitting can occur in both the CPT and the bright resonance spectra. Next, we will discuss the transformation of the absorption spectrum in detail based on the analytical expressions for the system obtained in Sec. III and the population distributions showed in Fig. 6.

As the φ increases, it is obtained that $H|b\rangle \neq 0$, i.e., the laser-induced transitions out of the state $|b\rangle$ turned off by the completely destructive interference is opened. Then, under the action of the laser, the population is transferred from the state $|b\rangle$ to $|a\rangle$ and $|c\rangle$, resulting in the increase of the population in $|a\rangle$ and $|c\rangle$ and the Hanle absorption near the center. Meanwhile, R_L^{out} is no longer zero and increases as the φ increases. Therefore, according to Eq. (31), the b-absorption channel opens and begins to contribute to the absorption as shown by the green dotted lines in Fig. 5, which leads to a faster decrease of the dips and a more remarkable increase of the central peak in the total absorption spectrum. In addition, the points of the minima in the absorption spectrum move away from $\Delta = \pm\Omega_T/\sqrt{2}$ with the increase of φ. According to Eq. (31), we can conclude that the positions of the minima satisfy

$$\Delta = \pm\frac{\Omega_T\sqrt{3\Gamma_L\cos 4\varphi - 4(6\Gamma_L + 3\Gamma_g + 2\gamma)\cos 2\varphi + 21\Gamma_L + 16\Gamma_g + 8\gamma}}{2\sqrt{(3\Gamma_L + 6\Gamma_g + 2\gamma)\cos 2\varphi - 3\Gamma_L - 4\Gamma_g - 2\gamma}}. \tag{37}$$

Substituting $\varphi = 0$ into the above formula yields $\Delta = \pm\Omega_T/\sqrt{2}$, which is consistent with the discussion in the previous section. When the TMF deviates from the direction perpendicular to the light polarization, we can see that the positions of the minima become dependent on the dissipation rates of ground states, the rate of laser-induced transitions, and the magnitude and the direction of the TMF. Therefore, when using the scheme introduced in Sec. IV A to the measurement of the magnetic field, Eq. (37) can serve as a good correction.

Then, we prove that when φ satisfies the bounds

$$\frac{1}{3} \leqslant \cos 2\varphi \leqslant 1 - \frac{2\Gamma_g}{3\Gamma_L + 6\Gamma_g + 2\gamma}, \tag{38}$$

the dips disappear and the absorption spectrum exhibits a single peak structure shown in Figs. 5(c) and 5(d), so that the dark resonance is entirely transformed into the bright resonance by changing the direction of the TMF.

From Fig. 6 we see that as the angle φ increases, the population difference between the dressed states $|b\rangle$ and $|a\rangle$ ($|c\rangle$) gradually decreases. And when increasing the angle φ to break the low bound of Eq. (38), that is,

$$\cos 2\varphi < \tfrac{1}{3}, \tag{39}$$

the populations in the states $|a\rangle$ and $|c\rangle$ begin to exceed that in the state $|b\rangle$ near $\Delta = 0$. It can be shown that when the Zeeman splitting satisfies

$$\Delta = \pm\Omega_T\sqrt{\frac{1 - 3\cos 2\varphi}{2}}, \tag{40}$$

the laser-induced transition rates between the three dressed states $|a\rangle$, $|b\rangle$, $|c\rangle$ are equal, i.e., $R_L^{\text{in}} = R_L^{\text{out}}$. Therefore, the population is equally distributed among the dressed states under the action of the laser field [see Eq. (29)] and the system is in the maximally mixed state in the subspace of the ground-state Zeeman sublevels [see Eq. (30)]. Under this condition, one can see from the analytical expression Eq. (31) for the absorption spectrum that the contributions of the three dressed states to the absorption are equal and the strongest absorption appears, that is,

$$\alpha_{\max} = \frac{4}{3(\Gamma + 2\Gamma^*)}, \tag{41}$$

so two maximum absorption peaks appear in the spectrum of the bright resonance [see Figs. 5(e) and 5(f)]. We note that the difference from the CPT dips near $\varphi = 0$ is that the amplitude of the peaks is independent of the ground-state relaxation processes and their positions only depend on the magnitude and direction of the TMF [see Eq. (40)] since the maximally mixed state is immune to the effect of population redistribution caused by the collisional and the transit processes. These features are suitable for the measurement of the magnetic field vector.

In addition, when $\varphi = 90^\circ$, we can see from Eq. (27) that at $\Delta = 0$, the two channels for the laser-induced transitions from $|b\rangle$ to $|a\rangle$ and from $|b\rangle$ to $|c\rangle$ are completely constructive, i.e., $R_L^{\text{out}} = 2\Gamma_L$, and the two channels for the laser-induced transitions from $|a\rangle$ to $|b\rangle$ and from $|c\rangle$ to $|b\rangle$ are completely destructive, i.e., $R_L^{\text{in}} = 0$. In this case, the population in the state $|b\rangle$ reaches the minimum (see Fig. 6) and only the b-absorption channel remains, so that the amplitude of the absorption reaches the minimum (see Fig. 5)

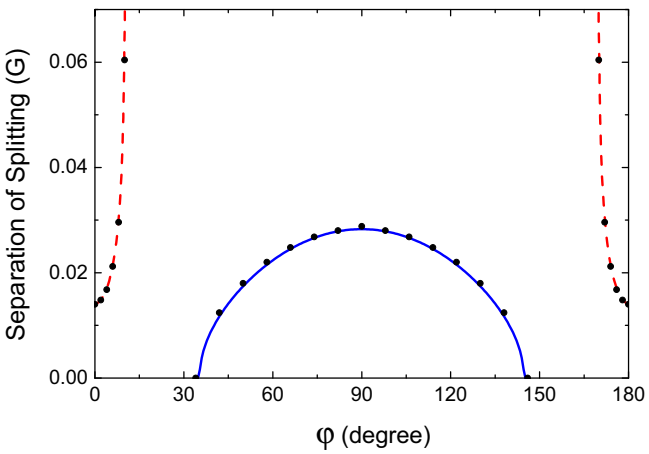

FIG. 7. The separation of the splitting in the absorption spectrum plotted as the function of the angle φ for the same parameters as in Fig. 3(a). The red dashed line and the blue solid line represent, respectively, the splittings of the CPT resonance and the bright resonance, and the black solid dots represent the exact numerical results.

$$\alpha_{\min} = \frac{4}{3(\Gamma + 2\Gamma^*)}\frac{9\Gamma_g + 4\gamma}{16\Gamma_L + 9\Gamma_g + 4\gamma}. \tag{42}$$

Meanwhile, the maximum absorption occurs at the position where condition Eq. (39) is satisfied, so we can see both the maximum absorption double peaks and the minimum absorption dip in Fig. 5(f).

In order to clearly demonstrate the dependence of the separ-
ation of the splitting in the direction of the TMF, we plot the separation of the splitting as the function of the angle φ in Fig. 7. The red dashed line and the blue solid line represent the splittings of the CPT resonance and the bright resonance, respectively, and they are in good agreement with the exact numerical results indicated by the black solid dots. In the blank regions, the absorption spectrum exhibits a single peak structure. We note that the absorption spectrum varies as a function of the angle φ with a periodicity of 180° and is symmetrical about $\varphi = 90^\circ$. In practice, the direction of the TMF can be reversed by measuring the separation of the splitting according to Eqs. (37) and (40). In addition, one can also take two orthogonal experiments to ensure that the signal of the bright resonance can always be observed in all angles. Therefore, it is possible to design a vector magnetometer based on these effects. Moreover, in the region of the bright resonance indicated by the blue solid line, since the peaks of the absorption spectrum correspond to the maximally mixed states, their positions and amplitudes are insensitive to the dissipation rates of the ground states and the separation of the splitting only depends on the magnitude and direction of the TMF. These features can contribute to measure the magnetic field more precisely and conveniently.

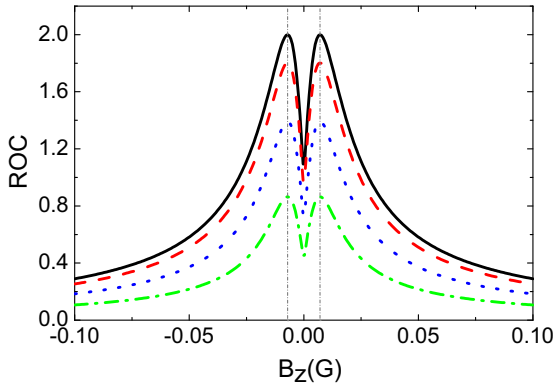

FIG. 8. In the case of $\varphi = 0^\circ$, the ROC of the ground states in the bare-state representation plotted as a function of the Zeeman splitting for several different values of $\Gamma_g = 0$ (black solid line), $\Gamma_g = 0.25\Gamma_g'$ (red dashed line), $\Gamma_g = \Gamma_g'$ (blue dotted line), $\Gamma_g = 3\Gamma_g'$ (green dash-dotted line) where $\Gamma_g' = 10^{-5}\Gamma$, $\gamma = \Gamma_g$ and the other parameters are the same as in Fig. 3(a). We can see that with the decrease of the dissipation rates of the ground states, the curve of the ROC gradually approaches one of the corresponding pure states and the positions of the maxima are maintained.

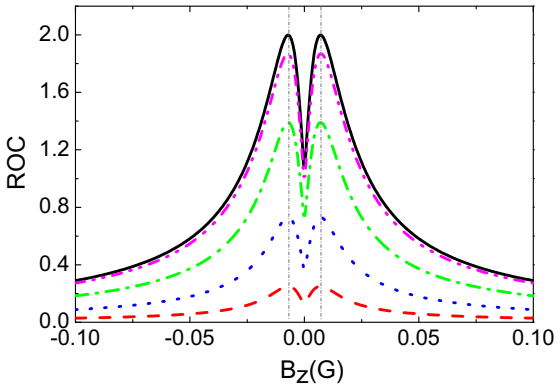

FIG. 9. In the case of $\varphi = 0^\circ$, the ROC of the ground states in the bare-state representation plotted as a function of the Zeeman splitting for $\Gamma_g = \gamma = 0$ (black solid line) and several different values of the Rabi frequencies $\Omega_L = 0.25\Omega_L'$ (red dashed line), $\Omega_L = 0.5\Omega_L'$ (blue dotted line), $\Omega_L = \Omega_L'$ (green dash-dotted line), $\Omega_L = 3\Omega_L'$ (magenta dash-dot-dotted line) where $\Omega_L' = 6\pi \times 10^6\ \mathrm{s}^{-1}$, and the other parameters are the same as in Fig. 3(a). We can see that with the increase of the magnitude of the light field, the curve of the ROC gradually approaches one of the corresponding pure states and the positions of the maxima are maintained.

V. ROBUSTNESS OF COHERENCE (ROC)

In Sec. IV A, we demonstrated that the ground-state relaxation processes play an important role in the absorption of the laser. According to the discussion for $\varphi = 0^\circ$, when these processes are so weak that they can be ignored (e.g., in a cold atom system), most of the population will be trapped in the dark state modulated by the Zeeman splitting, which will result in that the signal of the absorption is too weak to detect. In particular, when the rate of the collisional population redistribution is small compared to the rates of the laser-induced transitions and the transit effect, the splitting in the absorption spectrum will become indiscernible as noted in Ref. [1]. Therefore, the applicability of this scheme to the measurement of the magnetic field is limited.

On the other hand, with the rapid development of quantum technologies, quantum coherence has been a renewed emphasis as the fundamental quantum resource. Based on a systematic resource-theory framework [23], an observable measure of quantum coherence, named robustness of coherence (ROC), has been proposed recently [30,31] and its observability of ROC has been demonstrated in different experimental systems [45,46]. This measure is defined as

$$\mathcal{C} = \min_{\tau\in\mathcal{D}} \left\{ s \geqslant 0 \mid \frac{\rho + s\tau}{1+s} = \delta \in \mathcal{I} \right\}, \tag{43}$$

which represents the minimum weight of another state τ such that its convex mixture with ρ yields an incoherent state δ. Here, $\mathcal{D}$ is the convex set of density operators acting on a d-dimensional Hilbert space, and $\mathcal{I}$ is the subset of the incoherent states.

Using the semidefinite program provided by Ref. [30], we plot the ROC of the ground states as the function of the scanning magnetic field in the case of $\varphi = 0^\circ$, as shown in Fig. 8. We can see that with the same parameters as in Fig. 3(a), the shape of the ROC spectrum is similar to that of the absorption spectrum ignoring the reversal of the sign, and the splitting with the same separation appears near the center. As the dissipation rates of the ground states decrease, more population is accumulated into the dark states, so that the curve of the ROC gradually approaches one of the corresponding pure states and the splitting becomes more obvious. When the ground-state relaxation processes vanish, the values of the ROC at the two peaks reaches the maximum 2 for the three-dimensional state since all the population is accumulated into the maximally coherent states, and the contrast of the ROC spectrum is largest. In addition, although the coherence of the system is changed with different dissipation rates, the maxima always appear symmetrically at $\Delta = \pm\Omega_T/\sqrt{2}$ in which the corresponding dark states are the maximally coherent states. Therefore, by constructing the corresponding optimal witness [30,31], the ROC spectrum can be measured, and the magnitude of the TMF can be derived from the separation between the two maxima.

The dissipation rates of the ground states depend on conditions such as the temperature and the vapor density, which are often difficult to control. Meanwhile, the distribution of the population in the dark state $|b\rangle$ can also be adjusted by changing the magnitude of the light field according to Eq. (34). We can see from Fig. 9 that as the magnitude of the light field increases, the curve of the ROC approaches one of the pure states and the positions of the maxima are maintained, which is consistent with the previous theoretical analyses. These are similar to the effects of changing the dissipation rates of the ground states, but it is clear that the magnitude of the light field is easier to control. Therefore, this may provide a scheme for the measurement of the magnetic field which is complementary to that based on the absorption signal of the laser.

On the other hand, considering the corresponding relationship between the absorption and the quantum state of

the system as mentioned in Sec. IV A and the similarity between the spectral structures of the absorption and the ROC, the absorption of the laser is expected to be used to estimate coherence measures of an unknown quantum states. And compared to some previous measurement schemes of the coherence, this scheme is easier to implement.

VI. CONCLUSION

We have analytically studied the absorption spectra of a realistic closed transition, $F_g = 1 \rightarrow F_e = 0$ of the D_2 line of ^{87}Rb, excited resonantly by a linearly polarized laser in the presence of a TMF. We have found that when the TMF is perpendicular to the light polarization, the system is in a dark state modulated by the Zeeman splitting. Due to the effect of population redistribution caused by the ground-state relaxation processes, some of population can escape from the dark state, resulting in the absorption of the laser. When the dark states are modulated into the maximally coherent state of the Zeeman sublevel space, the population is equally distributed in each ground-state sublevel. In this condition, the impact of the collisional population redistribution is minimum, so that the system has the minimum deviation from the dark state. Therefore, two symmetrical dips appear in the absorption spectrum, and the separation between them is proportional to the magnitude of the TMF.

Further, we have studied the case where the angle between the TMF and the light polarization is arbitrary. We have found that by changing the direction of the TMF, the dark resonance can be transformed into a bright resonance. Moreover, when the angle meets certain conditions, the maximum absorption peaks appears in pairs, which correspond to the maximally mixed state. Since the maximally mixed state is immune to the effect of population redistribution caused by the ground-state relaxation processes, the amplitude of the peaks keeps a constant independent of these processes and the separation between the two maxima is only determined by the magnitude and direction of the TMF. Therefore, this scheme can be used for the measurement of the magnetic-field vector.

Whether decreasing the dissipation rates of the ground states or increasing the magnitude of the light field, more population will be accumulated into the dark state of the system, which results in that the absorption signal is difficult to detect precisely. On the contrary, we have found that the change of the ROC spectrum is more obvious in the same conditions, and the same extreme points are maintained well. Therefore, in order to detect the magnitude of the magnetic field, one only needs to find the positions of the two maxima of the ROC spectrum. And since the maximum corresponds to the maximally coherent state whose ROC reaches the upper bound, we can conveniently construct the corresponding optimal witness to determine their positions. Therefore, this may provide a scheme for the measurement of the magnetic field which is complementary to that based on the absorption signal of the laser.

ACKNOWLEDGMENTS

This work was supported by the National Natural Science Foundation of China (Grants No. 11774118 and No. 11474119) and the Fundamental Research Funds for the Central Universities of MOE (Grant No. CCNU18CXTD01).

[1] L. Margalit, M. Rosenbluh, and A. D. Wilson-Gordon, Phys. Rev. A **87**, 033808 (2013).
[2] E. Arimondo, Prog. Opt. **35**, 257 (1996).
[3] F. Renzoni, W. Maichen, L. Windholz, and E. Arimondo, Phys. Rev. A **55**, 3710 (1997).
[4] A. Huss, R. Lammegger, L. Windholz, E. Alipieva, S. Gateva, L. Petrov, E. Taskova, and G. Todorov, J. Opt. Soc. Am. B **23**, 1729 (2006).
[5] K. Nasyrov, S. Cartaleva, N. Petrov, V. Biancalana, Y. Dancheva, E. Mariotti, and L. Moi, Phys. Rev. A **74**, 013811 (2006).
[6] Y. J. Yu, H. J. Lee, I. H. Bae, H. R. Noh, and H. S. Moon, Phys. Rev. A **81**, 023416 (2010).
[7] H. R. Noh and H. S. Moon, Phys. Rev. A **82**, 033407 (2010).
[8] R. S. Grewal and M. Pattabiraman, J. Phys. B **47**, 195501 (2014).
[9] E. Taskova, E. Alipieva, and G. Todorov, J. Phys.: Conf. Ser. **700**, 012015 (2016).
[10] E. Taskova, E. Alipieva, and G. Todorov, J. Phys. B **51**, 035005 (2018).
[11] R. S. Grewal and M. Pattabiraman, J. Phys. B **48**, 085501 (2015).
[12] N. Ram, M. Pattabiraman, and C. Vijayan, Phys. Rev. A **82**, 033417 (2010).
[13] E. Breschi and A. Weis, Phys. Rev. A **86**, 053427 (2012).
[14] F. Renzoni, S. Cartaleva, G. Alzetta, and E. Arimondo, Phys. Rev. A **63**, 065401 (2001).
[15] J. Dimitrijevic, A. Krmpot, M. Mijailovic, D. Arsenovic, B. Panic, Z. Grujic, and B. M. Jelenkovic, Phys. Rev. A **77**, 013814 (2008).
[16] N. Ram and M. Pattabiraman, J. Phys. B **43**, 245503 (2010).
[17] H. S. Moon and H. J. Kim, Opt. Express **22**, 018604 (2014).
[18] H. J. Kim and H. S. Moon, Opt. Express **19**, 168 (2011).
[19] R. S. Grewal and M. Pattabiraman, Eur. Phys. J. D **70**, 219 (2016).
[20] A. Weis, Y. Q. Shi, and Z. D. Gruji, Eur. Phys. J. D **71**, 80 (2017).
[21] M. O. Scully and M. S. Zubairy, *Quantum Optics* (Cambridge University Press, Cambridge, UK, 1997).
[22] M. Auzinsh, D. Budker, and S. M. Rochester, *Optically Polarized Atoms: Understanding Light-Atom Interactions*, 1st ed. (Oxford University Press, Oxford, 2010).
[23] T. Baumgratz, M. Cramer, and M. B. Plenio, Phys. Rev. Lett. **113**, 140401 (2014).
[24] S. J. Buckle, S. M. Barnett, P. L. Knight, M. A. Lauder, and D. T. Pegg, Opt. Acta **33**, 1129 (1986).
[25] V. R. Blok and G. M. Krochik, Phys. Rev. A **41**, 1517 (1990).
[26] S. E. Harris, Phys. Rev. Lett. **62**, 1033 (1989).
[27] O. A. Kocharovskaya and P. Mandel, Phys. Rev. A **42**, 523 (1990).

[28] M. O. Scully, S. Y. Zhu, and A. Gavrielides, Phys. Rev. Lett. **62**, 2813 (1989).
[29] D. V. Kosachiov, B. G. Matisov, and Y. V. Rozhdestvensky, J. Phys. B **25**, 2473 (1992).
[30] C. Napoli, T. R. Bromley, M. Cianciaruso, M. Piani, N. Johnston, and G. Adesso, Phys. Rev. Lett. **116**, 150502 (2016).
[31] M. Piani, M. Cianciaruso, T. R. Bromley, C. Napoli, N. Johnston, and G. Adesso, Phys. Rev. A **93**, 042107 (2016).
[32] D. M. Brink and G. R. Satchler, *Angular Momentum*, 3rd ed. (Clarendon, Oxford, 1994).
[33] J. L. Meunier, Eur. Phys. J. **8**, 114 (1987).
[34] A. D. Wilson-Gordon, Phys. Rev. A **48**, 4639 (1993).
[35] Z. Ficek and S. Swain, *Quantum Interference and Coherence* (Springer, New York, 2005).
[36] P. Meystre and M. Sargent, *Elements of Quantum Optics* (Springer, Berlin, 1991).
[37] J. S. Peng and G. X. Li, *Introduction to Modern Quantum Optics* (World Scientific, Singapore, 1998).
[38] J. I. Cirac, R. Blatt, P. Zoller, and W. D. Phillips, Phys. Rev. A **46**, 2668 (1992).
[39] P. Zhou and S. Swain, Phys. Rev. Lett. **77**, 3995 (1996); Phys. Rev. A **56**, 3011 (1997).
[40] J. S. Peng, G. X. Li, P. Zhou, and S. Swain, Phys. Rev. A **61**, 063807 (2000).
[41] S. Menon and G. S. Agarwal, Phys. Rev. A **59**, 740 (1999).
[42] R. W. Boyd, *Nonlinear Optics*, 2nd ed. (Academic, San Diego, 2003).
[43] G. Morigi, J. Eschner, and C. H. Keitel, Phys. Rev. Lett. **85**, 4458 (2000)
[44] M. Fleischhauer, A. Imamoglu, and J. P. Marangos, Rev. Mod. Phys. **77**, 633 (2005).
[45] Y. T. Wang, J. S. Tang, Z. Y. Wei, S. Yu, Z. J. Ke, X. Y. Xu, C. F. Li, and G. C. Guo, Phys. Rev. Lett. **118**, 020403 (2017).
[46] W. Q. Zheng, Z. H. Ma, H. Y. Wang, S. M. Fei, and X. H. Peng, Phys. Rev. Lett. **120**, 230504 (2018).